RSC Advances

PAPER

View Article Online
View Journal | View Issue



Cite this: *RSC Adv.*, 2019, **9**, 13269

# Spinel oxide $CoFe_2O_4$ grown on Ni foam as an efficient electrocatalyst for oxygen evolution reaction†

Shasha Zhu,[a] Jinglei Lei, *[a] Yonghan Qin,[a] Lina Zhang[a] and Lijuan Lu[b]

Received 9th March 2019
Accepted 18th April 2019

DOI: 10.1039/c9ra01802f

rsc.li/rsc-advances

The effect of the oxygen evolution reaction (OER) is important in water splitting. In this work, we develop sphere-like morphology spinel oxide $CoFe_2O_4$/NF by hydrothermal reaction and calcination, and the diameter of the spheres is about 111.1 nm. The $CoFe_2O_4$/NF catalyst exhibits excellent electrocatalytic performance with an overpotential of 273 mV at a current density of 10 mA $cm^{-2}$ and a Tafel slope of 78 mV $dec^{-1}$. The cycling stability of $CoFe_2O_4$/NF is remarkable, and it only increased by 5 mV at a current density of 100 mA $cm^{-2}$ after 3000 cycles. Therefore, this simple method to prepare $CoFe_2O_4$/NF can enhance the OER properties of electrocatalysts, which makes $CoFe_2O_4$/NF a promising material to replace noble metal-based catalysts for the oxygen evolution reaction.



## 1. Introduction

Electrochemical water splitting has been considered a viable approach to produce clean hydrogen fuel through the use of renewable energy. Electrochemical water splitting consists of two half reactions: the hydrogen evolution reaction (HER) of the cathode and the oxygen evolution reaction (OER) of the anode.[1–4] Due to the OER involving four-proton-coupled electron transfer and O=O band formation, the overpotential of the OER is higher than that of the HER in electrochemical water splitting, and the OER is the bottleneck of electrochemical water splitting.[5–11]

In order to reduce the overpotentials of the OER, efficient electrocatalysts with excellent catalytic activity and stability are needed. Noble metal-based materials like Ru- and/or Ir-based catalysts have been well-known as prominent catalysts for OER, but Ru- and/or Ir-based catalysts still require larger overpotential to deliver a current density of 10 mA $cm^{-2}$. Moreover, the scarcity, high cost and poor durability seriously hamper large-scale application of noble metal-based materials.[12–19]

Recently, due to the low cost and earth-abundant reserves, many efforts have been made to develop high activity non-noble metal based electrocatalysts. Non-noble transition metals such as Fe, Co, Ni and Mn have attracted a lot of attention, and the compounds of transition-metals have been suggested as replaceable electrocatalysts in OER. As OER catalysts, spinel oxides, such as N-CG–CoO,[20] $Co_3O_4$,[21] $Co_3O_4$/N-rmGO,[22] $LiCoO_2$,[23] $NiFeO_x$,[24] $NiCo_2O_4$ (ref. 25) and $CoFe_2O_4$ (ref. 26) have been widely studied as advanced electrocatalysts because of their unique crystal structure and remarkable properties. Among the various spinel oxides, $CoFe_2O_4$ is one of the most interesting compounds due to its high abundance, low cost, low toxicity, rich redox chemistry and high electrochemical activity. There are a few reports on the research of $CoFe_2O_4$ as an OER electrocatalyst.[27,28] Zhang *et al.* reported $CoFe_2O_4$ nanofibers which were prepared by electrospinning technique with an overpotential of 340 mV to deliver a current density of 10 mA $cm^{-2}$ in 1.0 M KOH.[26] Ding *et al.* prepared $CoFe_2O_4$/SWNTs nanorods *via* hydrothermal method and compound with SWNTs by sonication, which required an overpotential of 310 mV to achieve a current density of 10 mA $cm^{-2}$ in 1.0 M KOH.[28] The $CoFe_2O_4$/biomass carbon hybrid catalyst has been synthesized from sulfate reducing bacteria *via* enrichment of Co with porous structure and rough surfaces, and required 300 mV for generating the current density of 10 mA $cm^{-2}$ in 1.0 M KOH.[27] Although many advances have been made, the electrical conductivity and surface area are low, resulting in poor catalytic performance, and the catalytic performances need to be improved.[29]

In general, to ensure the electrocatalyst working at high electrochemical activity, the catalyst is usually attached to a conducting surface to ensure fast electron transport. The nickel foam (NF) has conductive surface with three-dimensional (3D) porous structure, and such 3D architecture is beneficial for increasing the number of reaction sites.[30,31] In this work we design sphere-like morphology spinel oxide $CoFe_2O_4$ grown on Ni foam (NF) through hydrothermal and calcination method using urea, iron chloride tetrahydrate, cobalt nitrate

[a]College of Chemistry and Chemical Engineering, Chongqing University, Chongqing 400044, China. E-mail: leijlei@163.com

[b]College of Computer Science and Technology, Chongqing University of Posts and Telecommunications, Chonqing 400065, China

† Electronic supplementary information (ESI) available: Additional experimental, additional FESEM images, cyclic voltammograms and tables. See DOI: 10.1039/c9ra01802f

hexahydrate and sodium chloride. During the process of hydrothermal, the sodium chloride not only acts as crystal template but also adjusts the morphology of the catalyst. The electrode has excellent electrochemical conductivity, small charge transfer resistance, large active surface area and outstanding stability.

## 2. Experimental

### 2.1 Chemicals

Ferrous chloride tetrahydrate ($FeCl_2 \cdot 4H_2O$, >99.7%) was obtained from Chemical Reagent factory of Tianjin. Cobalt nitrate hexahydrate ($Co(NO_3)_2 \cdot 6H_2O$, >98.5%), sodium chloride (NaCl, >99.5%) and urea ($CO(NH_2)_2$, >99.0%) were provided by Chemical Reagent factory of Chengdu Kelong. Ni foams (99.99% purity, 1.0 mm thickness, 110 PPI pore size) were purchased from Lifeixin Metal Co. Ltd. All the reagents were analytical grade and used without further purification.

### 2.2 Catalyst synthesis

The $CoFe_2O_4$/NF catalyst was synthesized by hydrothermal reaction and annealing treatment. Typically, NF (1 cm × 1 cm) was cleaned by sonication in acetone, 3.0 M HCl and ethanol for 5 min each to remove the surface oxide layer, the pre-cleaned NF was transferred into 30 mL of the mixture solution containing 0.5 mmol $Co(NO_3)_2 \cdot 6H_2O$, 1.0 mmol $FeCl_2 \cdot 4H_2O$, 3.0 mmol $CO(NH_2)_2$ and 3.0 mmol NaCl for 6 h at 120 °C. After hydrothermal reaction, rinsed the NF with distilled water and absolute ethanol to remove the residual reactants, and dried in vacuum oven for overnight. Finally, the NF was put into quartz boat, and the NF was annealed to 300 °C at 5 °C $min^{-1}$ in static argon environment for 1 h. For the comparison, the $CoO_x$/NF and $FeO_x$/NF were prepared by the same procedure without $FeCl_2 \cdot 4H_2O$ and $Co(NO_3)_2 \cdot 6H_2O$.

### 2.3 Catalysts characterization

The morphology and elemental mapping distribution of the samples were examined using a field-emission scanning electron microscope (FESEM) equipped with an energy dispersive spectrometer (EDS) (JEOL JSM-7800F, Japan). The phase composition of the samples was identified by using an X-ray diffractometer (XRD, X'pert PRO, PANalytical B.V., Holland) using Cu Kα radiation (0.15418 nm). The chemical composition of the sample was analyzed by X-ray photoelectron spectroscopy (XPS, Thermo electron ESCALAB250, USA) using Al Kα radiation.

### 2.4 Electrode preparation and electrochemical characterization

The measurement of electrochemical impedance spectroscopy was tested at 25 °C in a standard three-electrode system connected to an autolab (PGSTAT302N) electrochemical workstation, and other electrochemical measurements were performed with the three-electrode system using a CHI760B electrochemical workstation at 25 °C. The three-electrode system includes a sample coated on Ni foam as the working electrode, a graphite plate as the counter electrode and an Hg/HgO electrode as the reference electrode, respectively. Electrolyte of 1.0 M KOH aqueous solution was saturated with oxygen bubbles at least 30 min prior to experiment, and OER polarization curves were obtained by linear sweep voltammetry (LSV) with a scan rate of 5 mV $s^{-1}$. The resistance $R$ was tested by electrochemical impedance spectroscopy (EIS). EIS measurements were carried out in the configuration from the frequency range of $10^5$ to 0.1 Hz, and conducted under oxygen evolution voltage, which corresponds to the potential at 10 mA $cm^{-2}$. The stability test was performed by the cyclic voltammetry (CV) method with a scan rate of 40 mV $s^{-1}$.

## 3. Results and discussion

The crystal structure of $CoFe_2O_4$/NF was investigated by XRD, as shows in Fig. 1a. Selected area electron diffraction pattern at 44.507°, 51.846° and 76.370° reflect of NF to (111), (200) and (220) diffraction lattice faces, respectively. The prominent peaks at 30.0°, 35.4°, 37.3°, 43.5°, 53.9°, 57.2°, 62.7°, 65.7° and 77.8° are defined as the (220), (311), (222), (400), (422), (511), (440), (531) and (444) diffraction lattice faces, respectively, which are in good accordance with the standard patterns of $CoFe_2O_4$/NF.[32–35] X-ray photoelectron spectroscopy (XPS) was performed to classify the elemental compositions and chemical valences of $CoFe_2O_4$/NF (Fig. 1b–d). Fig. 1b displays the Co $2p_{3/2}$, Co $2p_{1/2}$ and satellite peaks for $Co^{3+}$ (779.3 and 794.8 eV), $Co^{2+}$ (781.6 and 794.8 eV) and satellite features (785.5 and 802.1 eV).[36,37] The peaks originated at 709.7, 711.8, 722.9 and 724.9 eV are attributed to $Fe^{2+}$ $2p_{3/2}$, $Fe^{3+}$ $2p_{3/2}$, $Fe^{2+}$ $2p_{1/2}$ and $Fe^{3+}$ $2p_{1/2}$ states, respectively (Fig. 1c).[38,39] Fig. 1d shows the high resolution O 1s spectrum, and the O 1s spectrum in Fig. 1d exhibited two peaks at 529.1 and 530.6 eV, which due to the metal–oxygen bonds and oxygen in the hydroxyl group on the outside of catalyst.[40–42] The XRD and XPS test results confirmed that the main component of the catalyst is the spinel oxide $CoFe_2O_4$.

The morphology of $CoFe_2O_4$/NF characterized by SEM. Fig. 2a shows that $CoFe_2O_4$/NF also retained the NF framework morphology, and the catalytic material of $CoFe_2O_4$/NF was uniformly grown on the surface of NF substrate (Fig. 2b). Fig. 2c revealed that the catalyst of $CoFe_2O_4$/NF displayed sphere-like structure. The sphere and sphere closely connected to more ideal sphere-like crystals of $CoFe_2O_4$/NF, and the diameter of the sphere is about 111.1 nm. The images of $CoFe_2O_4$/NF precursors were shown in Fig. S1 (ESI, ESI†). The morphology of precursor is the same as $CoFe_2O_4$/NF catalyst, which confirms that only the composition of the final catalyst is changed and the morphology don't change after calcination. During the formation of the spherical structure of the catalyst, NaCl acts as crystal template and plays a role in regulating the morphology. Using NaCl as crystal template has the following advantages: (i) it is one of the most soluble salts in water; (ii) the high melting point of NaCl ensures that the template does not collapse during calcination; (iii) NaCl is the most abundant salt on earth.[43–45] The carbonate and hydroxyl anions are provided by the hydrolysis of urea, which have an important effect on the anisotropy growth of the catalyst crystals.[46] The elemental maps

 

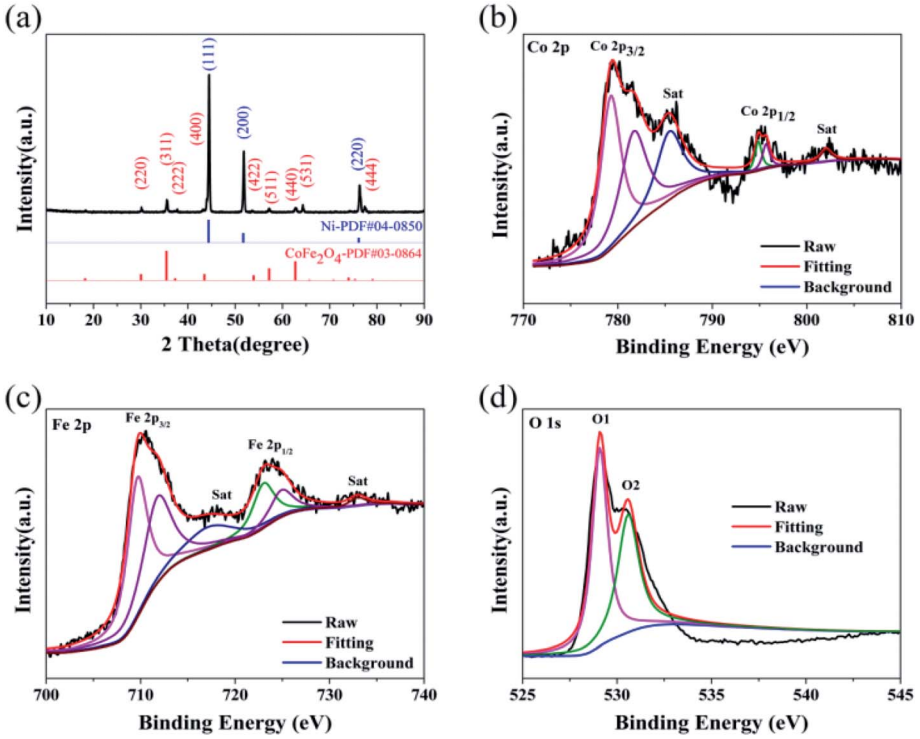


Fig. 1 (a) X-ray diffraction (XRD) pattern of $CoFe_2O_4$/NF; (b) high-resolution Co 2p XPS spectra for $CoFe_2O_4$/NF; (c) high-resolution Fe 2p XPS spectra for $CoFe_2O_4$/NF; (d) high-resolution O 1s XPS spectra for $CoFe_2O_4$/NF.

of $CoFe_2O_4$/NF were shown in Fig. 2d–f. The Fe, Co and O elements uniformly decorated with the NF substrate, which means that the catalyst of $CoFe_2O_4$/NF is successfully prepared and uniformly grown on the NF substrate.

The OER performances of $CoFe_2O_4$/NF, $CoO_x$/NF and $FeO_x$/NF were assessed in 1.0 M KOH (Fig. 3a). The overpotentials at 10, 50 and 100 mA $cm^{-2}$ for $CoFe_2O_4$/NF are 273, 341 and 400 mV, respectively, while the overpotentials of $CoO_x$/NF ($FeO_x$/NF) are 317 (360) mV, 413 (449) mV and 478 (529) mV at the current density of 10, 50 and 100 mA $cm^{-2}$, respectively (Table S1†).These results demonstrate that the $CoFe_2O_4$/NF is superior to $CoO_x$/NF and $FeO_x$/NF in activity. The Tafel slope for

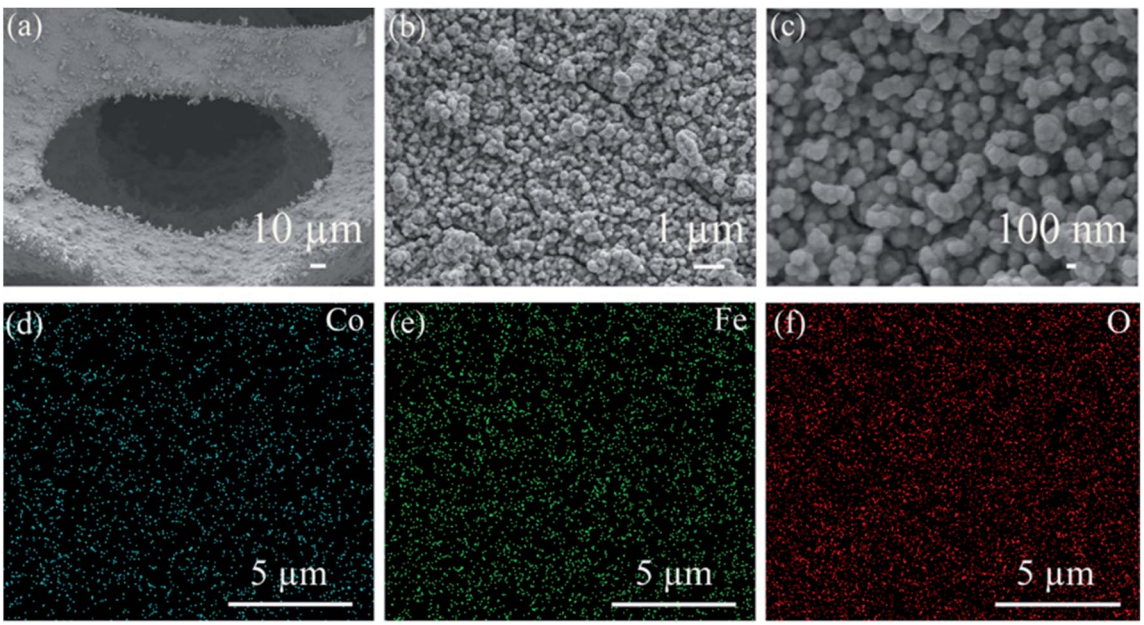


Fig. 2 (a)–(c) FESEM images of $CoFe_2O_4$/NF at different magnifications. (d)–(f) The elemental mapping of the $CoFe_2O_4$/NF.

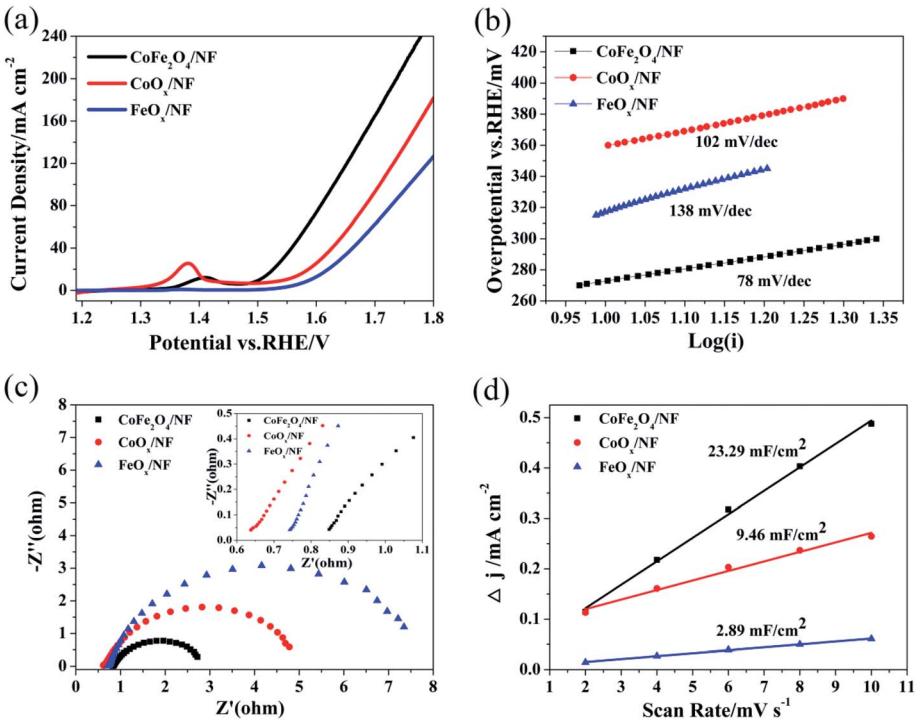


Fig. 3 (a) The OER polarization curves of $CoFe_2O_4$/NF, $CoO_x$/NF and $FeO_x$/NF in 1.0 M KOH. (b) The corresponding Tafel plots of $CoFe_2O_4$/NF, $CoO_x$/NF and $FeO_x$/NF in 1.0 M KOH. (c) Nyquist plot representations of the electrochemical impedance spectra of $CoFe_2O_4$/NF, $CoO_x$/NF and $FeO_x$/NF. (d) Linear fitting of the capacitive currents *versus* scan rate obtained from cyclic voltammetry tests for $CoFe_2O_4$/NF, $CoO_x$/NF and $FeO_x$/NF.

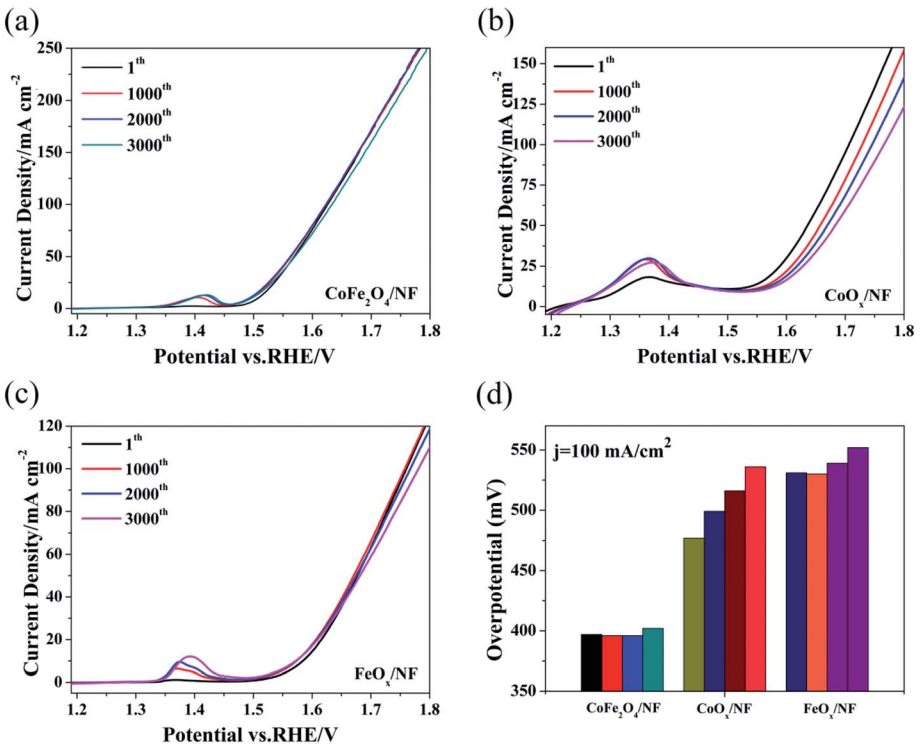


Fig. 4 The cycling stability of catalysts $CoFe_2O_4$/NF (a), $CoO_x$/NF (b) and $FeO_x$/NF (c), (d) for the above polarization curve, the corresponding overpotential of 100.00 mA $cm^{-2}$.

$CoFe_2O_4$/NF is 78 mV $dec^{-1}$, which is smaller than that of $CoO_x$/NF (102 mV $dec^{-1}$) and $FeO_x$/NF (138 mV $dec^{-1}$), indicating that $CoFe_2O_4$/NF has a more favorable OER kinetics.[47] To investigate the kinetics leading to the catalytic enhance, electrochemical impedance spectroscopy (EIS) was used. Fig. 3c shows that the charge transfer resistance ($R_{ct}$) values of the $CoFe_2O_4$/NF, $CoO_x$/NF and $FeO_x$/NF are estimated to be 2.08, 4.49 and 7.24 Ω from the diameter of semicircle, respectively, so the $CoFe_2O_4$/NF catalyst has smaller $R_{ct}$ than $CoO_x$/NF and $FeO_x$/NF, and the $CoFe_2O_4$/NF catalyst has rapider reaction rate during the catalytic process.[48] Fig. 3d shows the double-layer capacitance ($C_{dl}$) to evaluate the ECSA. The $C_{dl}$ is obtained by CV measurement, and CV measurement is recorded at different scan rates: from 2 mV $s^{-1}$ to 10 mV $s^{-1}$ (Fig. S2†). The $C_{dl}$ value of $CoFe_2O_4$/NF (23.29 mF $cm^{-2}$) is much higher than those of $CoO_x$/NF (9.46 mF $cm^{-2}$) and $FeO_x$/NF (2.89 mF $cm^{-2}$), indicating that $CoFe_2O_4$/NF own much higher ECSA than $CoO_x$/NF and $FeO_x$/NF.[49] The OER catalytic performance of $CoFe_2O_4$/NF is compared with reported $CoFe_2O_4$ catalysts, as in Table S2.†

The test method for cycling stability is CV with the scan rate of 40 mV $s^{-1}$ for 3000 cycles, and Fig. 3a–c show the OER polarization curves of $CoFe_2O_4$/NF, $CoO_x$/NF and $FeO_x$/NF at different sweeping cycles. The overpotential of $CoFe_2O_4$/NF was mostly retained up to 3000 cycles, and the overpotential of $CoFe_2O_4$/NF at the current density of 100 mA $cm^{-2}$ only increased 5 mV after cycling for 3000 cycles. However, the overpotential of $CoO_x$/NF and $FeO_x$/NF investigation of cycling stability is further proved that the catalyst increased 21 and 16 mV at the current density of 100 mA $cm^{-2}$, respectively. The $CoFe_2O_4$/NF has excellent stability.[50–52] The superior OER performance of $CoFe_2O_4$/NF can be explained to the following factors: (i) the sphere morphology of $CoFe_2O_4$/NF can expose rich edge active sites; (ii) the binder-free catalyst and beneficial contacts between $CoFe_2O_4$/NF and NF can provide low resistance pathways for electrons (Fig. 4).

## 4. Conclusions

In this work, spinel oxide $CoFe_2O_4$ was successfully prepared on NF substrate by hydrothermal reaction and calcination. In the process of hydrothermal, NaCl not only acts as crystal template but also plays a role in regulating the morphology, and the addition of urea is beneficial to the anisotropic growth of the catalyst crystal. The morphology of $CoFe_2O_4$ on NF substrate is sphere-like, and the diameter of the sphere is about 111.1 nm. Electrochemical tests showed that $CoFe_2O_4$/NF has excellent catalytic activity toward OER, and $CoFe_2O_4$/NF catalyst delivered current density of 10 mA $cm^{-2}$ at overpotential of 273 mV. Moreover, the catalyst of $CoFe_2O_4$/NF has outstanding cycling stability and the overpotential of the $CoFe_2O_4$/NF at the high current density of 100 mA $cm^{-2}$ almost stable after 3000 cycles CV stability test. As a result, the $CoFe_2O_4$/NF catalyst showed improved OER performance due to the decreased charge transfer resistance and increased number of active sites to the reference sample. These results make $CoFe_2O_4$/NF a promising material to replace noble metal-based catalysts for OER.

## Conflicts of interest

There are no conflicts to declare.

## Acknowledgements

This study was supported by the Project No. CDJXS11221171 supported by the Fundamental Research Funds for the Central Universities, and the sharing fund of Chongqing University's Large-scale Equipment. We also thank Dr Jianxin He for improving the analysis of X-ray photoelectron spectroscopy. We would also like to acknowledge the reviewers and editor for helpful feedback and ideas for improving the quality of our manuscript.

## References

1 Y. Li, L. Hu, W. Zheng, X. Peng, M. Liu, P. K. Chu and L. Y. S. Lee, *Nano Energy*, 2018, **52**, 360–368.
2 Y. Liu, X. Liang, L. Gu, Y. Zhang, G.-D. Li, X. Zou and J.-S. Chen, *Nat. Commun.*, 2018, **9**, 2609.
3 A. Pirkarami, S. Rasouli and E. Ghasemi, *Appl. Catal., B*, 2019, **241**, 28–40.
4 J.-T. Ren, G.-G. Yuan, C.-C. Weng, L. Chen and Z.-Y. Yuan, *Nanoscale*, 2018, **10**, 10620–10628.
5 S. Shit, S. Chhetri, W. Jang, N. C. Murmu, H. Koo, P. Samanta and T. Kuila, *ACS Appl. Mater. Interfaces*, 2018, **10**, 27712–27722.
6 Y. Teng, X.-D. Wang, J.-F. Liao, W.-G. Li, H.-Y. Chen, Y.-J. Dong and D.-B. Kuang, *Adv. Funct. Mater.*, 2018, **28**, 1802463.
7 H. Wu, T. Yang, Y. Du, L. Shen and G. W. Ho, *Adv. Mater.*, 2018, **30**, 1804341.
8 W. Xi, G. Yan, Z. Lang, Y. Ma, H. Tan, H. Zhu, Y. Wang and Y. Li, *Small*, 2018, **14**, 1802204.
9 H. Xu, B. Wang, C. Shan, P. Xi, W. Liu and Y. Tang, *ACS Appl. Mater. Interfaces*, 2018, **10**, 6336–6345.
10 D. Zhong, L. Zhang, C. Li, D. Li, C. Wei, Q. Zhao, J. Li and J. Gong, *J. Mater. Chem. A*, 2018, **6**, 16810–16817.
11 Z. Ma, H. Fu, C. Gu, Y. Huang, S. Hu, Q. Li and H. Wang, *RSC Adv.*, 2018, **8**, 28209–28215.
12 F. Jing, Q. Lv, J. Xiao, Q. Wang and S. Wang, *J. Mater. Chem. A*, 2018, **6**, 14207–14214.
13 V. R. Jothi, R. Bose, H. Rajan, C. Jung and S. C. Yi, *Adv. Energy Mater.*, 2018, **8**, 1802615.
14 Y. Li, F.-M. Li, X.-Y. Meng, X.-R. Wu, S.-N. Li and Y. Chen, *Nano Energy*, 2018, **54**, 238–250.
15 G. Ren, Q. Hao, J. Mao, L. Liang, H. Liu, C. Liu and J. Zhang, *Nanoscale*, 2018, **10**, 17347–17353.
16 X. Wang, W. Ma, C. Ding, Z. Xu, H. Wang, X. Zong and C. Li, *ACS Catal.*, 2018, **8**, 9926–9935.
17 Z. Zhang, X. Ma and J. Tang, *J. Mater. Chem. A*, 2018, **6**, 12361–12369.
18 X. Zheng, Y. Zhang, H. Liu, D. Fu, J. Chen, J. Wang, C. Zhong, Y. Deng, X. Han and W. Hu, *Small*, 2018, **14**, 1803666.
19 J. Wang, L. Li, L. Meng, L. Wang, Y. Liu, W. Li, W. Sun and G. Li, *RSC Adv.*, 2018, **8**, 35131–35138.

20 S. Mao, Z. Wen, T. Huang, Y. Hou and J. Chen, *Energy Environ. Sci.*, 2014, **7**, 609–616.
21 J. Zhao, Y. He, Z. Chen, X. Zheng, X. Han, D. Rao, C. Zhong, W. Hu and Y. Deng, *ACS Appl. Mater. Interfaces*, 2019, **11**, 4915–4921.
22 Y. Liang, Y. Li, H. Wang, J. Zhou, J. Wang, T. Regier and H. Dai, *Nat. Mater.*, 2011, **10**, 780–786.
23 T. Maiyalagan, K. A. Jarvis, S. Therese, P. J. Ferreira and A. Manthiram, *Nat. Commun.*, 2014, **5**, 3949.
24 C. C. L. McCrory, S. Jung, J. C. Peters and T. F. Jaramillo, *J. Am. Chem. Soc.*, 2013, **135**, 16977–16987.
25 W. Q. Zaman, W. Sun, M. Tariq, Z. Zhou, U. Farooq, Z. Abbas, L. Cao and J. Yang, *Appl. Catal., B*, 2019, **244**, 295–302.
26 Z. Zhang, J. Zhang, T. Wang, Z. Li, G. Yang, H. Bian, J. Li and D. Gao, *RSC Adv.*, 2018, **8**, 5338–5343.
27 S. Bi, J. Li, Q. Zhong, C. Chen, Q. Zhang and Y. Yao, *RSC Adv.*, 2018, **8**, 22799–22805.
28 Y. Ding, J. Zhao, W. Zhang, J. Zhang, X. Chen, F. Yang and X. Zhang, *ACS Appl. Energy Mater.*, 2018, **2**, 1026–1032.
29 H. Xu, J. Wei, M. Zhang, C. Liu, Y. Shiraishi, C. Wang and Y. Du, *Nanoscale*, 2018, **10**, 18468–18472.
30 Y. Li, S. Yang, H. Li, G. Li, M. Li, L. Shen, Z. Yang and A. Zhou, *Colloids Surf., A*, 2016, **506**, 694–702.
31 J. Liang, Y. Wang, C. Wang and S. Lu, *J. Mater. Chem. A*, 2016, **4**, 9797–9806.
32 W. Bian, Z. Yang, P. Strasser and R. Yang, *J. Power Sources*, 2014, **250**, 196–203.
33 S. Li, S. Sirisomboonchai, A. Yoshida, X. An, X. Hao, A. Abudula and G. Guan, *J. Mater. Chem. A*, 2018, **6**, 19221–19230.
34 Y. Xu, W. Bian, J. Wu, J.-H. Tian and R. Yang, *Electrochim. Acta*, 2015, **151**, 276–283.
35 W. Yan, W. Bian, C. Jin, J.-H. Tian and R. Yang, *Electrochim. Acta*, 2015, **177**, 65–72.
36 C. Mahala, M. D. Sharma and M. Basu, *Electrochim. Acta*, 2018, **273**, 462–473.
37 Y. Niu, X. Huang, L. Zhao, W. Hu and C. M. Li, *ACS Sustainable Chem. Eng.*, 2018, **6**, 3556–3564.
38 Y. Wang, Q. Liu, T. Hu, L. Zhang and Y. Deng, *Appl. Surf. Sci.*, 2017, **403**, 51–56.
39 Y. Wang, Q. Liu, L. Zhang, T. Hu, W. Liu, N. Liu, F. Du, Q. Li and Y. Wang, *Int. J. Hydrogen Energy*, 2016, **41**, 22547–22553.
40 W. Yan, X. Cao, J. Tian, C. Jin, K. Ke and R. Yang, *Carbon*, 2016, **99**, 195–202.
41 T. Zhang, Z. Li, L. Wang, Z. Zhang and S. Wang, *Int. J. Hydrogen Energy*, 2019, **44**, 1610–1619.
42 S. C. Sekhar, G. Nagaraju and J. S. Yu, *Nano Energy*, 2018, **48**, 81–92.
43 S. Xiong, J. S. Chen, X. W. Lou and H. C. Zeng, *Adv. Funct. Mater.*, 2012, **22**, 861–871.
44 W. Wang, W. Chen, P. Miao, J. Luo, Z. Wei and S. Chen, *ACS Catal.*, 2017, **7**, 6144–6149.
45 G. Fu, Z. Liu, J. Zhang, J. Wu, L. Xu, D. Sun, J. Zhang, Y. Tang and P. Chen, *Nano Res.*, 2016, **9**, 2110–2122.
46 B. Wang, T. Zhu, H. Wu, R. Xu, J. Chen and X. Lou, *Nanoscale*, 2012, **4**, 2145–2149.
47 Z.-Q. Jiang, Y.-F. Li, X.-J. Zhu, J. Lu, L. Zhang and T. Wen, *RSC Adv.*, 2018, **8**, 38562–38565.
48 T. G. Novak, O. Prakash, A. P. Tiwari and S. Jeon, *RSC Adv.*, 2019, **9**, 234–239.
49 F. Wang, J. Zhao, W. Tian, Z. Hu, X. Lv, H. Zhang, H. Yue, Y. Zhang, J. Ji and W. Jiang, *RSC Adv.*, 2019, **9**, 1562–1569.
50 H. Lin, N. Liu, Z. Shi, Y. Guo, Y. Tang and Q. Gao, *Adv. Funct. Mater.*, 2016, **26**, 5590–5598.
51 P. S. Toth, M. Velicky, M. A. Bissett, T. J. Slater, N. Savjani, A. K. Rabiu, A. M. Rakowski, J. R. Brent, S. J. Haigh, P. O'Brien and R. A. W. Dryfe, *Adv. Mater.*, 2016, **28**, 8256–8264.
52 Y. Guo, L. Gan, C. Shang, E. Wang and J. Wang, *Adv. Funct. Mater.*, 2017, **27**, 1602699.